Soils and Foundations 2012;52(3):511–523

The Japanese Geotechnical Society

Soils and Foundations

www.sciencedirect.com
journal homepage: www.elsevier.com/locate/sandf

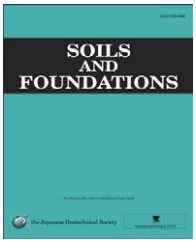

Mechanical characterisation of the fouled ballast in ancient railway track substructure by large-scale triaxial tests

Viet Nam Trinh[a,b], Anh Minh Tang[a], Yu-Jun Cui[a,*], Jean-Claude Dupla[a], Jean Canou[a], Nicolas Calon[b], Lucie Lambert[b], Alain Robinet[b], Olivier Schoen[c]

[a]*Ecole des Ponts ParisTech, Laboratoire Navier/CERMES, France*
[b]*Direction of Engineering—SNCF, France*
[c]*RFF, France*

Available online 8 June 2012

Abstract

In the track substructure of ancient railways in France, a fouled ballast layer has often been created with time. The mechanical behaviour of this coarse soil was studied in the laboratory using a large-scale triaxial cell. The soil taken from the fouled ballast layer of an ancient railway was re-compacted to a dry density of 2.01 Mg/m^3 at three water contents (4, 6, and 12%) corresponding to three values of the initial degree of saturation (32, 48, and 100% respectively). Both monotonic and cyclic triaxial tests were performed under constant water content conditions. The experimental results gave the following evidence of the significant effect of the water content on the soil mechanical behaviour: (i) the lower the compaction water content, the higher the shear strength; (ii) a permanent axial strain of 0.4% was found after a large number of cycles at a water content of 4%, while it was 1.4% at the higher water content of 6%. For the saturated soil specimen, failure was even observed after a limited number of cycles. Based on the results obtained, a constitutive model for permanent deformation was elaborated, that accounts for the stress level, the number of cycles and the soil water content.

Keywords: Fouled ballast; Railway track substructure; Large-scale triaxial test; Cyclic behaviour; Water content effects; Constitutive modelling

1. Introduction

A fouled ballast layer refers to a layer within the railway track substructure, located in between the ballast and the subgrade soil (UIC, 2003). For the new high-speed lines in France, a sub-ballast layer or capping layer has been designed and constructed according to the technical specifications of the French National Railway Company (SNCF, 2006). By contrast, in the substructure of ancient railway tracks, there is no such sub-layer and a fouled ballast layer was created naturally. After Fortunato et al. (2010), the formation of this layer can be attributed to various mechanisms, for example, grain size modification in ballast particles due to cracking, weathering or crushing, the infiltration of materials from the surface, the infiltration of materials from an underlying layer, and the weathering of the sleepers. In order to respect the new requirements corresponding to the increase in load and the speed of trains, numerous ancient railway lines have been modernised, repaired or rehabilitated in France. Preliminary investigations conducted at different sites show that poor drainage was the major cause of track deterioration.

*Correspondence to: Ecole des Ponts—ParisTech, Laboratoire Navier/CERMES, 6-8 Avenue Blaise Pascal, Cité Descartes, Champs-sur-Marne, 77455 Marne-La-Vallée, France. Tel.: +33 1 64 15 35 50; fax: +33 1 64 15 35 62.
E-mail address: yujun.cui@enpc.fr (Y.-J. Cui).
Peer review under responsibility of The Japanese Geotechnical Society.

Production and hosting by Elsevier

0038-0806 © 2012 The Japanese Geotechnical Society. Production and hosting by Elsevier B.V. All rights reserved.
http://dx.doi.org/10.1016/j.sandf.2012.05.009

Nomenclature

C_u	coefficient of uniformity
c	apparent cohesion
D	diameter of specimen
d	diameter of grain
d_{max}	maximum diameter of grain
d_x	diameter of grain defined by x% passing grain size
N	number of cycles
q	deviator stress
q_{max}	maximum deviator stress
Δq	amplitude of cyclic deviator stress
Δq_{max}	maximum amplitude of cyclic deviator stress
p	mean stress
Δp	amplitude of cyclic mean stress
Δp_{max}	maximum amplitude of cyclic mean stress
S_r	degree of saturation
S_{ri}	initial degree of saturation
w	water content
OMC	optimal moisture content
ε_1	axial strain
ε_1^p	permanent axial strain
ε_1^r	reversible axial strain
ε_1^p(N)	permanent axial strain at N cycles
ε_1^{p*}(N)	permanent axial strain from 100 cycles to N cycles
ε_v	volumetric strain
ε_{vmax}	maximum volumetric strain
ε_v^p	permanent volumetric strain
φ	friction angle
υ	Poisson's ratio
σ_3	confining pressure

For this reason, a drainage system has been installed systematically (SNCF, 2006) in spite of the extra costs. On the other hand, it has been observed that some substructures of ancient railways in excavation zones without drainage systems do not show any stability problems, indicating the necessity of optimising the design of drainage systems. Actually, the railway platform stability is closely related to the mechanical sensibility of the fouled ballast to variations in the water content; thus, it is obviously necessary to better understand its hydro-mechanical behaviour.

Large-scale triaxial tests are usually carried out to study the mechanical behaviour of ballast-based materials under static and cyclic loading. Most works have been performed on ballast (Raymond and Williams, 1978; Stewart, 1986; Raymond and Bathurst, 1994; Indraratna et al., 1998; Suiker et al., 2005; Lackenby et al., 2007; William and Peter, 2008), while a few works have been carried out on sub-ballast (Suiker et al., 2005). The test results show that under cyclic loading, these materials tend to compact. This compaction behaviour generally causes an increase in the mechanical strength and stiffness. Generally, after a large number of loading cycles, the resilient behaviour stabilizes, but the permanent strain increases (Kalcheff and Hicks, 1973; Brown, 1974; Li and Selig, 1994; Selig and Water, 1994; Gidel et al., 2001; Malla and Joshi, 2008; Ekblad, 2008). According to Selig and Water (1994), failure induced by the accumulation of plastic strain under repeated loads takes place when the material becomes saturated or when the drainage capacity is insufficient. This shows the significant effects of the water content and the drainage conditions on the mechanical behaviour.

The influence of the water content on the permanent deformation of Unbound Granular Materials (UGM) was studied by Gidel et al. (2002), Ekblad (2006), and Werkmeister et al. (2003). The results show that the water content strongly affects the resilient modulus and the permanent deformation under cyclic loading; increasing the water content causes a reduction in the resilient modulus and an increase in the permanent deformation. These kinds of studies on the hydro-mechanical behaviour of coarse-grained materials for railway application remain rare.

In constitutive modelling, the permanent deformation is usually predicted by accounting for the stress level (Shenton, 1974; Lekarp and Dawson, 1998) or the number of cycles (Barksdale, 1972; Paute et al., 1988; Sweere, 1990; Hornych et al., 1993; Wolff and Visser, 1994). Gidel et al. (2001) proposed a model to predict the permanent deformation of UGM as a function of both the stress level and the number of loading cycles based on the results of triaxial tests with a multi-stage loading procedure. Pérez et al. (2006) also proposed a model accounting for the effects of both the stress level and the number of cycles, but the experimental data considered for the model calibration were from the cyclic triaxial tests following a standard procedure, i.e., single-loading stage procedure.

In the present paper, the effects of the water content of the fouled ballast on its shear strength parameters and permanent deformation were investigated by carrying out both monotonic and cyclic triaxial tests. Based on the results obtained and the model presented by Gidel et al. (2001), a constitutive model was elaborated, allowing the determination of permanent strain by taking into account the stress level, the number of load cycles, and the water content.

2. Soil studied

The soil studied was taken from Sénissiat (North-West of Lyon, France), located along an ancient line from Bourg-en-Bresse to Bellegarde. At the moment of sampling, the line was being rehabilitated; the ballast layer had been removed for this purpose. Fig. 1 presents a picture taken during the sampling. A visual examination shows a 0.3-m fouled ballast

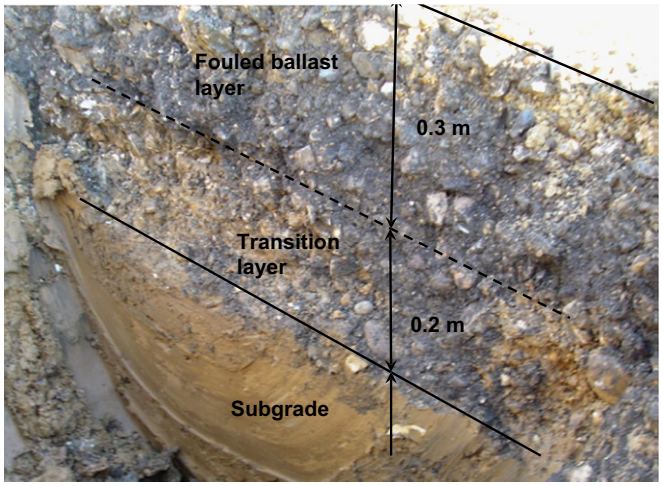

Fig. 1. Picture taken during sampling.

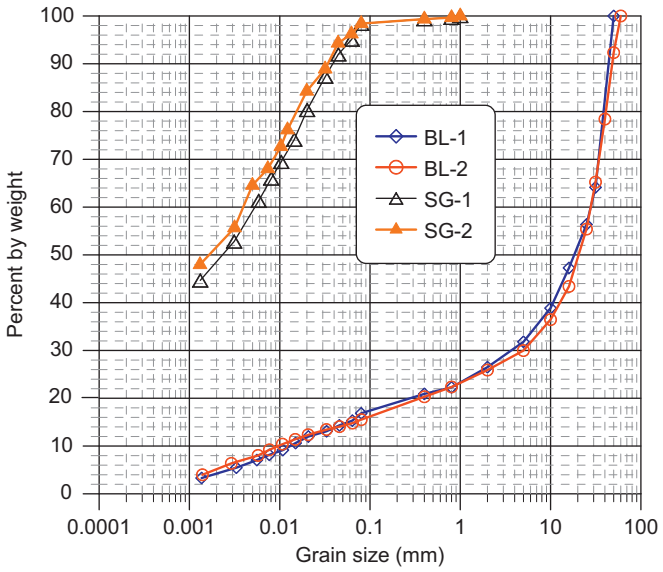

Fig. 2. Grain-size distribution curves of the fouled ballast (BL) and the subgrade (SG).

layer constituted of well-mixed coarse-/fine-grained soil, a 0.2-m transition layer constituted of a mixture of more finely grained soil, and the subgrade. The fouled ballast and the subgrade were excavated by a mechanical shovel and transported in large bags for the laboratory testing.

Geotechnical identification tests were performed on both soils taken from the fouled ballast layer and the subgrade (Trinh et al., 2011). The Atterberg limits, blue methylene value, and mineralogy were determined on the fine-grained portion (< 100 μm), whereas an analysis of the grain-size distribution on both the fouled ballast layer and the subgrade soils covered the whole grain elements of different dimensions. The grain-size distribution curves obtained are shown in Fig. 2. Two tests have been performed on the fouled ballast (BL-1 and BL-2) and two others on the subgrade (SG-1 and SG-2). It can be observed that the subgrade contains mainly fine particles (< 0.080 mm), of which 50% are clay-size particles (< 0.002 mm). The fouled ballast corresponds to a heterogeneous material constituted of large-size elements (up to 60 mm) and fine particles. It is composed of ballast, stones of 25–60 mm (44%) in dimension, sand, degraded ballast, and fine grains from the subgrade soil (56%). The clay fraction (< 0.002 mm) in the fouled ballast is 5%. The main geotechnical parameters of these two soils, after being passed through a 100-μm sieve, are given in Table 1.

To investigate the compaction properties of the fouled ballast, modified Proctor compaction was carried out on the portion sieved at 20 mm. The results are shown in Fig. 3, in which the dry density obtained is plotted versus the moulding water content. The maximum dry density and the optimum moisture content (OMC) of the fouled ballast sieved through the 20-mm sieve are 1.97 Mg/m^3 and 8.8%, respectively. This compaction curve was then extended to the fouled ballast with the whole grain elements following the method described in the French standard (AFNOR, 1999) for the compaction of coarse-grained soils. The results obtained show a maximum dry density of 2.28 Mg/m^3 at an OMC of 4.4%. This value is slightly lower than the dry

Table 1
Geotechnical parameters of fine-grained portion ($d < 100$ μm) of the fouled ballast and the subgrade.

Parameter	Soil type (fine-grained $d < 100$ μm)	
	Fouled ballast	Subgrade
Fine-grained portion ($d < 100$ μm): (%)	18	98
Liquid limit (w_L): (%)	45.7	57.8
Plastic limit (w_p): (%)	30.9	33.7
Plasticity index (I_p): (%)	14.8	24.1
Blue methylene value (g)	3.6	6.2
Carbonates content (%)	16	0

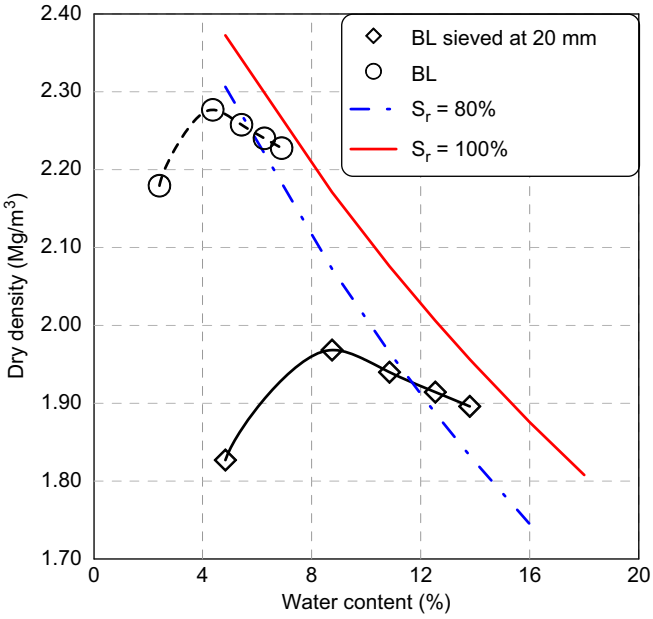

Fig. 3. Modified Proctor compaction curves.

density of the fouled ballast layer measured in the field (2.39 Mg/m^3) by Trinh et al. (2011). From the compaction curve shown in Fig. 3, it can be noted that there is only one data point on the dry side of the optimum water content. This lack of data might lead to inaccurate maximum dry density values, and can be explained by the limited quantity of soil taken from the site.

3. Experimental methods

A large-scale triaxial device, developed by Dupla et al. (2007), was used. A schematic view of the device is shown in Fig. 4. This large-scale triaxial apparatus allows the consolidation and the shear of soil specimens, 300 mm in diameter and 600 mm in height. Vertical monotonic and cyclic loads can be applied, by controlling either the displacement or the force, using a 500-kN hydraulic actuator. The confining pressure is applied either through a simple mechanical regulating valve and air–water interface or through a dynamic pressure control device. The whole device is controlled by a digital system. For cyclic loadings, the system can apply a large number of cycles (up to several million) at a frequency of several tens of Hz (depending on the displacement amplitude). A displacement transducer (LVDT), integrated to the hydraulic actuator, allows the monitoring of the piston displacement, and thereby, the determination of the vertical strain of the specimen. The volumetric strain of the specimen is obtained by considering the cell's outgoing or incoming water volume, using a high-precision scale or based on the displacement of the confining hydraulic actuator.

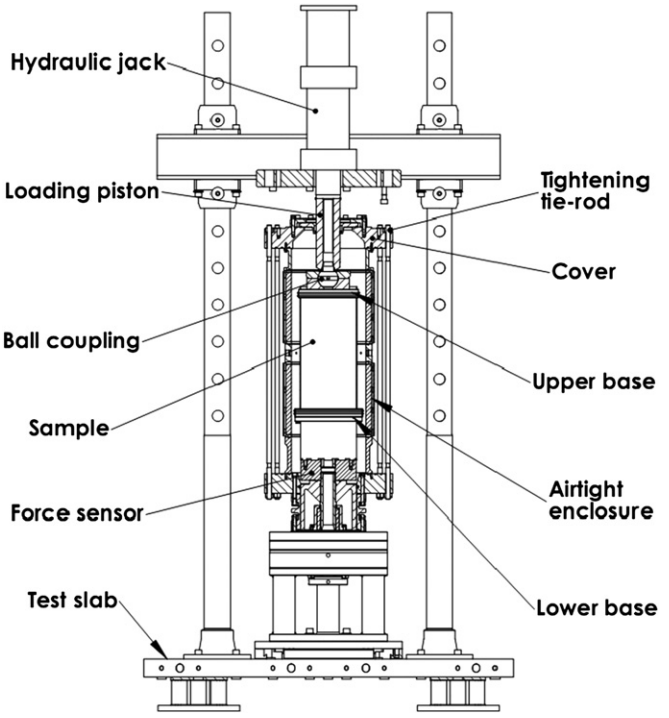

Fig. 4. Schematic view of the large triaxial apparatus.

According to the grain-size distribution curves of the fouled ballast (Fig. 2), the largest grain size is 60 mm. If a sample size ratio is defined as the diameter of triaxial specimen D divided by maximum particle dimension d_{max}, this ratio is equal to 5 ($D=300$ mm and $d_{max}=60$ mm). According to AFNOR (1994), as the soil is not uniform with $C_u=d_{60}/d_{10}=900$, the effects of the sample size can be ignored.

The soil sample was prepared by compaction. Prior to compaction, the fouled ballast taken from the field was first air-dried, ground, wetted by the spraying of distilled water to reach the target water content, and finally stored in a hermetic plastic box for homogenisation of the soil moisture. The compaction was performed at least 48 h after the soil humidification. The soil specimen was compacted in six layers of 100 mm in a metallic mould using a vibrating hammer. The dry density of the soil was controlled based on the thickness of each layer and the mass of the soil. The final dry density of the soil specimens was 2.01 Mg/m^3 (88% of the maximum dry density). This value corresponds to the maximum density obtained by this compaction method. After compaction, the sample in its mould was first put on the lower base of the triaxial cell. Then, the mould was removed to complete the sample installation procedure.

In order to have an idea about the compression behaviour of this material, static compression was also carried out in a large-scale oedometer cell (300 mm in diameter) on a sample compacted following the same procedure as previously described, but to a lower dry density ($\rho_d=1.64$ Mg/m^3 and $e=0.63$). The compaction was performed using a 50-t mechanical press. The results are shown in Fig. 5. A pre-consolidation pressure of 22 kPa can be identified, reflecting the effect of the initial compaction. It can also be observed that a vertical stress of 700 kPa was necessary to reach a void ratio of 0.33, which corresponds to a dry density of 2.01 Mg/m^3 (value for triaxial samples).

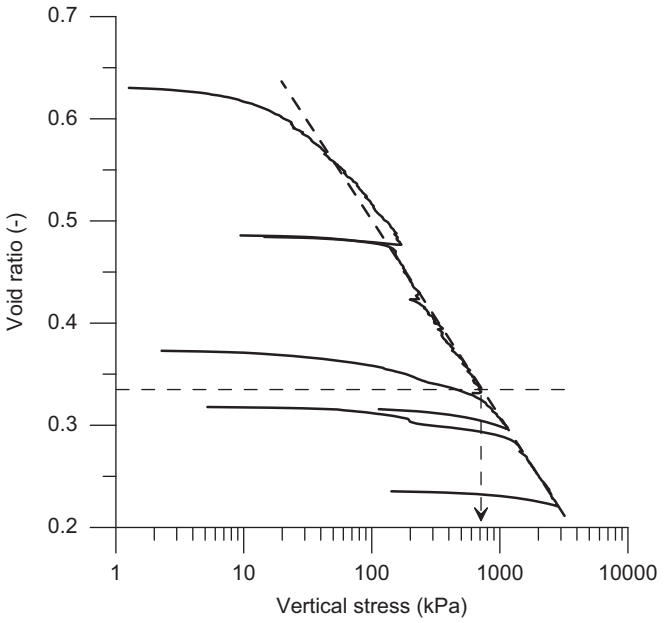

Fig. 5. Static compression curve.

Monotonic drained triaxial tests were first performed in order to determine the shear strength parameters at various water contents. The results obtained were then analysed to define the loading stages in the cyclic triaxial tests. The multi-stage loading procedure used by Gidel et al. (2001) was applied in the cyclic tests. After the installation of the triaxial cell, a confining pressure of $\sigma_3=30$ kPa was first applied. This value is close to the horizontal stress estimated in the field conditions and is much lower than the vertical compaction stress (700 kPa) estimated from Fig. 5. The maximum shear stress (q_{max}) was increased in stages, keeping a constant ratio of $\Delta q/\Delta p=3$. The frequency used, 5 Hz, corresponds to the frequency measured in situ for a train speed of 100 km/h (typical for the trains circulating on the old railways in France, SNCF, 2009).

4. Experimental results

4.1. Monotonic triaxial tests

Five tests were performed at a water content of 4% and two tests were performed on the saturated soil specimens. For the tests at a water content of 4%, shearing was performed under four values of confining pressure, $\sigma_3=30$, 100, 200, and 400 kPa, for four tests, TS1, TS2, TS3 and TS4, respectively, the test under $\sigma_3=30$ kPa being duplicated for a repeatability study (test TS5). The results of these tests are shown in Fig. 6, in which the deviator stress (q) and the volumetric strain (ε_v) are plotted versus the axial strain (ε_1). The results of the duplicated tests (TS1 and TS5) are quite similar, showing the good repeatability of the experimental technique. It is also believed that the results of the triaxial tests may not be significantly affected by the sample compaction conditions. The effect of confining pressure on the shearing behaviour is quite common for this range in stress, i.e., the higher the confining pressure, the higher the maximum deviator stress. Contractancy is observed for confining stress higher than 200 kPa, whereas dilatancy is observed for lower confining pressures.

The results of the tests performed under a confining pressure of 100 kPa and at two different water contents (4 and 12%) are shown in Fig. 7. A significant effect of the water content on the mechanical behaviour of the soil can be observed, i.e., the shear strength of the drier specimen (TS2, $w=4\%$) is twice as that of the saturated specimen (TS6, $w=12\%$). Moreover, for the drier specimen (TS2), contractancy is followed by dilatancy during shearing, while mere contractancy is observed for the saturated specimen (TS6). In Fig. 8, the results of the tests performed under a confining pressure of 400 kPa are shown for the two water contents. The effect of the water content can be also clearly observed, but it is less significant than in the case of the lower confining pressure (Fig. 7). The drier specimen (TS4, $w=4\%$) shows a higher shear strength ($q_{max}=1535$ kPa) and a lower volume change ($\varepsilon_{vmax}=3.32\%$), while these values are $q_{max}=1304$ kPa and $\varepsilon_{vmax}=5.05\%$ for the saturated specimen (TS7, $w=12\%$), respectively.

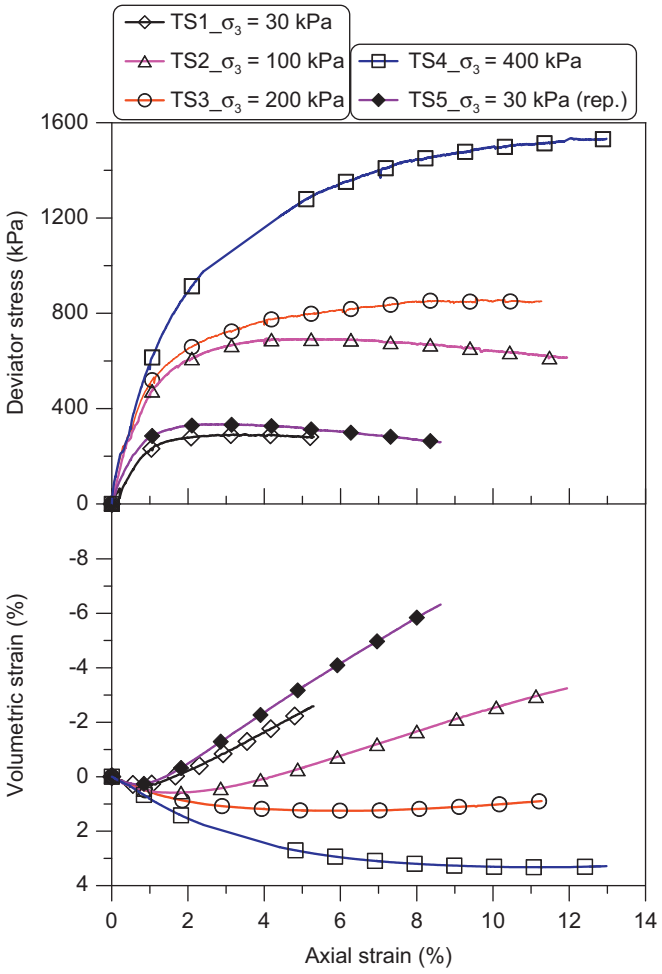

Fig. 6. Monotonic compression triaxial tests at various confining pressures—results of the tests at a water content of 4%.

For further analysis, the deviator stress at failure is defined as either the peak deviator stress, for the tests under low confining pressures ($\sigma_3 \leq 100$ kPa), or the deviator stress, at an axial strain of 12% where the mode of failure is characterised by "bulging" (Indraratna et al., 1998) in the case of higher confining pressures. Fig. 9 presents the failure envelopes at water contents of 4 and 12% (saturated) in the p–q plane. From this figure, the shear strength parameters can be determined, i.e., friction angle $\varphi=39^\circ$ for $w=4\%$ and 37° for the saturated state and apparent cohesion $c=60$ kPa for $w=4\%$ and 22 kPa for the saturated state.

4.2. Cyclic triaxial tests

The stress paths were defined based on the results of the monotonic triaxial tests (Fig. 10). The main idea was to have three or four cyclic loading stages before reaching failure. In the tests, after applying a confining pressure of 30 kPa, which is close to the in situ mean stress, cyclic loading was applied by varying shear deviator q from 0 to q_{max} at a constant stress ratio of $\Delta q/\Delta p=3$. The value of q_{max} was then increased at the end of each stage. The levels of stress chosen depended, as a consequence, on the stress distribution in the railway track

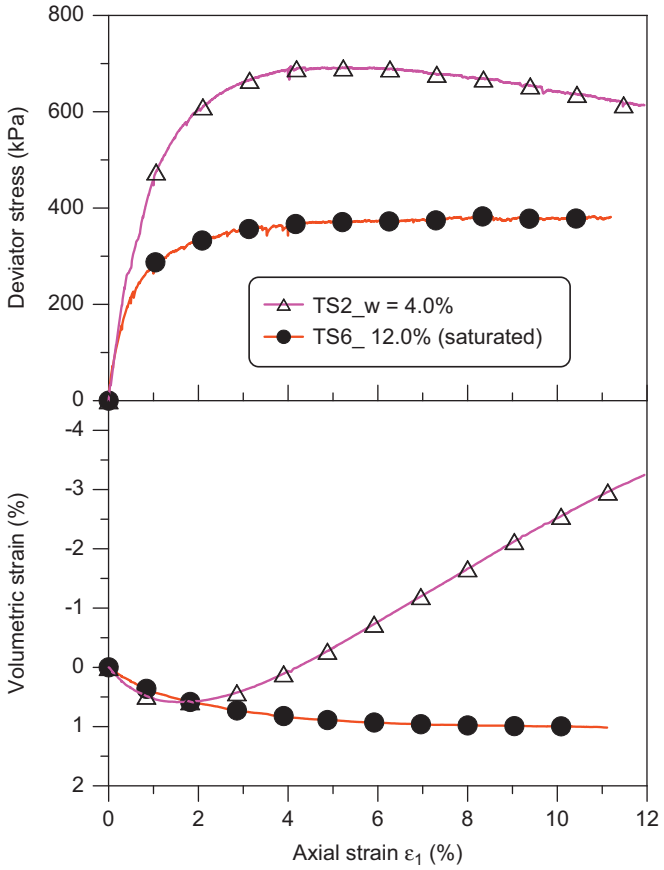

Fig. 7. Monotonic compression triaxial tests at two water contents (w=4 and 12%)—results of the tests at a confining pressure of 100 kPa.

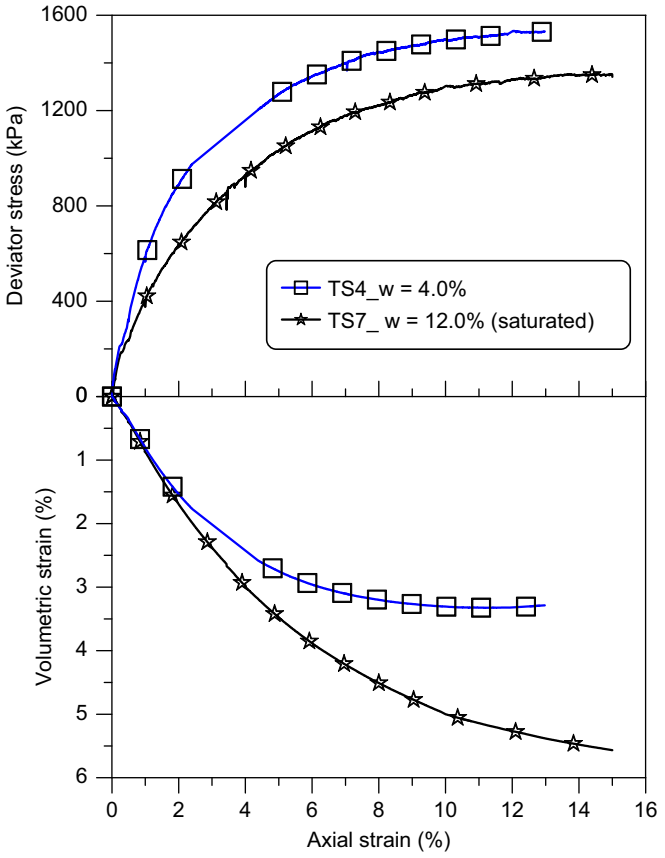

Fig. 8. Monotonic compression triaxial tests at two water contents (w=4 and 12%)—results of the tests at a confining pressure of 400 kPa.

substructure and the peak strength determined from the monotonic triaxial tests. Note that the stress distribution within the fouled ballast layer depends on the wheel load, the dimensions of the sleeper, the thickness of the ballast layer, and the weight of the above materials (ballast, rail, and sleeper). The wheel load applied by trains in France is about 16–22 t per axle (Alias, 1984); the thickness of the ballast layer varies from 250 to 600 mm. The maximum vertical stress at the surface of the fouled ballast layer can then be estimated at 40–90 kPa. This value is comparable with that observed for Indian Railways (Jain and Keshav, 1999) and American Railways (Selig and Water, 1994; Yang et al., 2009). Note, however, that in other countries where heavier wagons are used, the wheel load may reach 30 t per axle (Alias, 1984). This corresponds to a vertical stress of 120–140 kPa on the fouled ballast layer (Li and Selig, 1998; Jain and Keshav, 1999; Gräbe and Clayton, 2009). By considering a Poisson's coefficient of ν=0.4 for the fouled ballast of the old railways in France (Selig and Water, 1994), the mean horizontal stress is estimated at 30 kPa. This value has been regarded as the confining pressure for all the cyclic triaxial tests. Four values were chosen for q_{max} (q_{max}=45, 90, 140, and 200 kPa) corresponding to the four loading stages (see Fig. 10). For each of the first three stages, 30,000 cycles were applied. For the last stage, several hundred thousand cycles were applied. Three tests were performed for three values of

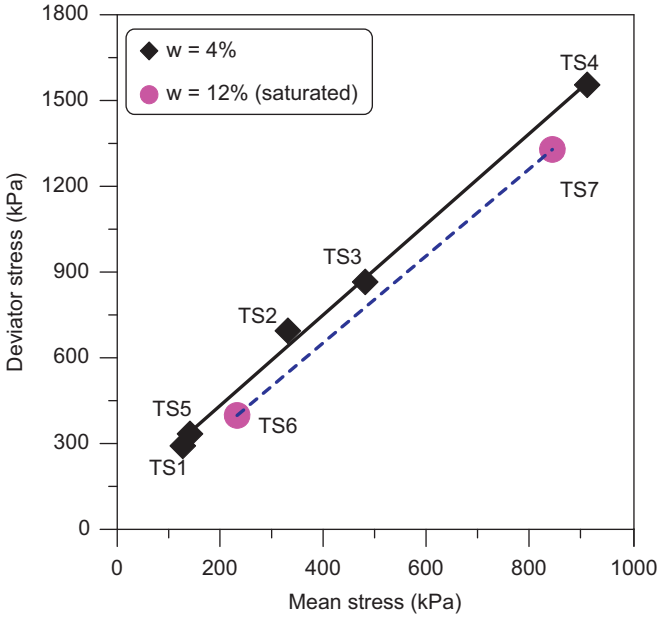

Fig. 9. Failure envelopes at w=4 and 12% (saturated) in the q–p plane.

water content, w=4, 6, and 12%, corresponding to the three values of the initial degree of saturation, S_{ri}=32, 49, and 100%, respectively. Note that the specific gravity was

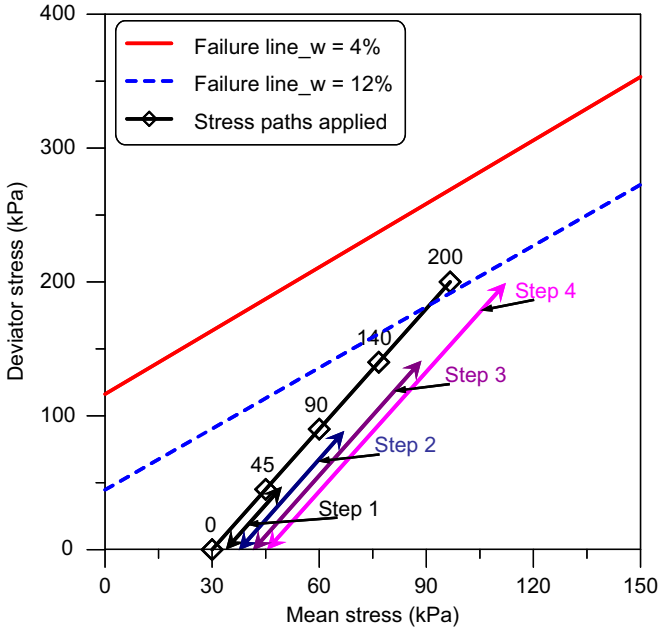

Fig. 10. Loading paths for the cyclic triaxial tests.

determined separately for particles smaller and larger than 2 mm. The values obtained are identical, i.e., 2.68 Mg/m^3. This value was used to calculate the degree of saturation.

The results obtained from the test at $w=4\%$ (TC1), during the first ten cycles, are shown in Fig. 11. The deviator stress, q, varies following a sinusoidal function between 0 and the maximum value of $q_{max}=45$ kPa (Fig. 11a). The axial strain also changes accordingly in a cyclic fashion (Fig. 11b). Two distinct parts can be identified on the axial strain curve, a reversible part, ε_1^r, and an irreversible part, ε_1^p. The reversible strain remains fairly constant, while the irreversible strain or permanent strain increases with the loading cycles at a rate that tends to decrease with an increasing number of cycles. This is in agreement with the observation by O'Reilly and Brown (1991), and can be explained by the work-hardening effect or density-increase effect. The variations in volumetric strain (Fig. 11c) are similar to the variations in axial strain.

The results of test TC1 ($w=4\%$) are shown in Fig. 12 for all four loading stages. Except for the first three stages, where 30,000 cycles were applied in each stage, 900,000 cycles were applied in the last stage under a maximum deviator stress of $q_{max}=200$ kPa (Fig. 12a). The permanent axial and volumetric strains are also presented in Fig. 12b and c, respectively. The significant effect of the stress level on the permanent strain can be observed; the permanent axial strain increases with an increasing deviator stress, and moreover, its stabilisation is less and less evident with an increasing deviator stress. For the first stage, $q_{max}=45$ kPa, the permanent axial strain stabilises after 30,000 cycles. For the other stages at higher deviator stresses, the permanent axial strain still keeps increasing after 30,000 cycles. For the last stage, the permanent strain increases quickly during the first cycles and then slows down with an increasing number of cycles. The volumetric

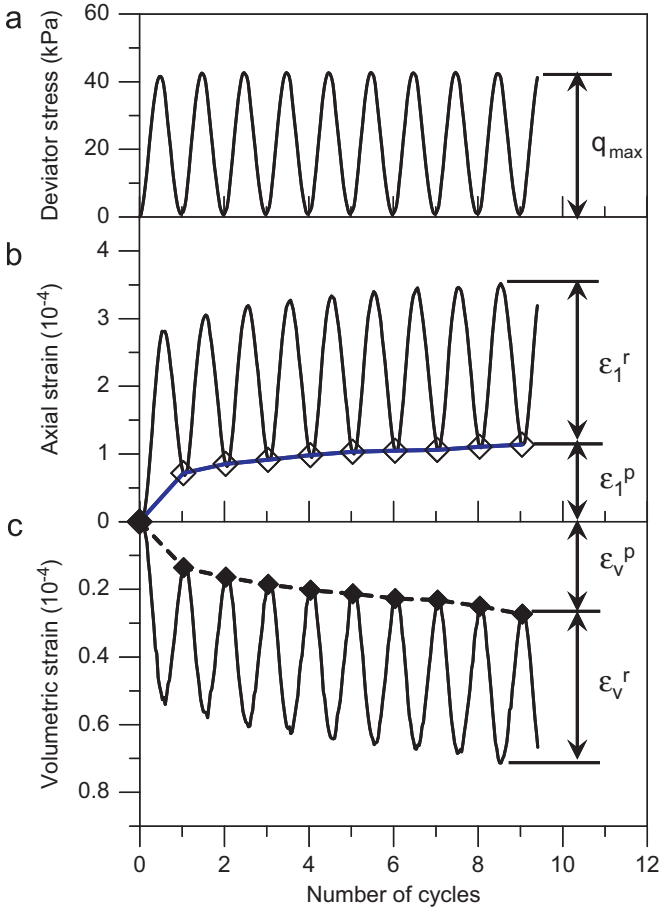

Fig. 11. Cyclic triaxial tests—results obtained for test TC1 ($w=4\%$) during the first ten cycles.

strain was determined using a device that consists of a piston located in a small cylindrical chamber connected to the cell. Since this measurement depends on the confining pressure, the frequency, and the water tightness of the system, it was quite difficult to ensure satisfactory accuracy. For this reason, in further analyses, only the permanent axial strain will be considered.

The results of the three cyclic triaxial tests are shown in Fig. 13, where the permanent axial strain is plotted versus the number of cycles for each loading stage. For the first stage (Fig. 13a), $q_{max}=45$ kPa, the test at a water content of 4% (TC1) shows a quick increase in permanent axial strain during the first cycles. Stabilisation is reached at 2.5×10^{-4} after 1000 cycles. For the test at a water content of 6% (TC2), the permanent axial strain also increases quickly and then stabilises after 5000 cycles at 3.5×10^{-4}. The stabilisation of the permanent axial strain is not observed for test TC3 at $w=12\%$, even after 30,000 cycles. The permanent axial strain reaches 7.5×10^{-4} at the end of the first loading stage (Fig. 13a).

For the second and the third stages (Fig. 13b and c, respectively), the following phenomena can be observed: (i) the permanent axial strain increases quickly during the first cycles and then slows down at larger numbers of cycles; (ii) no stabilisation of permanent axial strain is observed even after

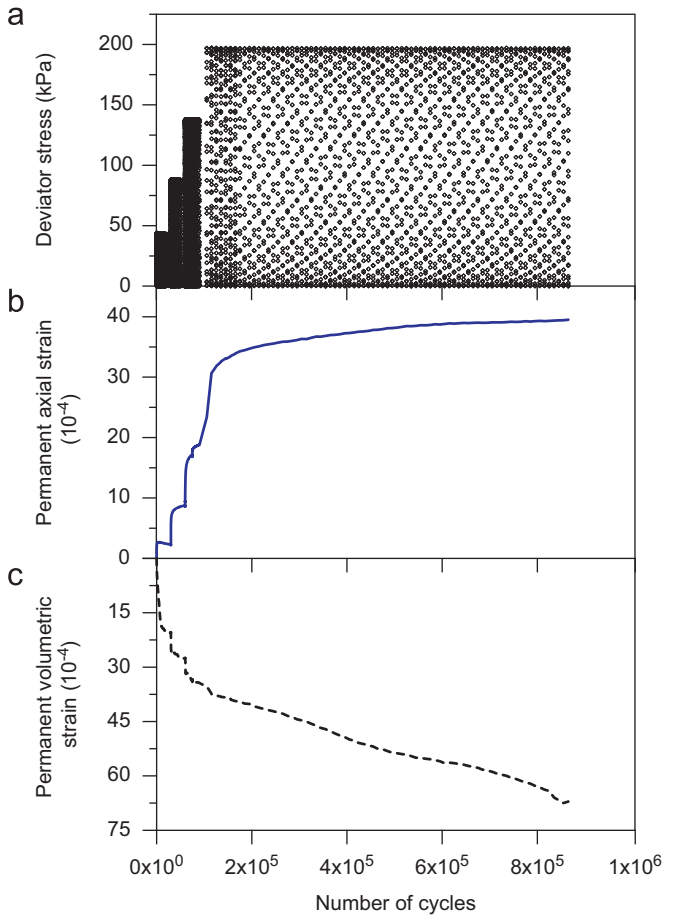

Fig. 12. Cyclic triaxial tests—results obtained for test TC1 (w=4%) during the whole test.

30,000 cycles; (iii) the higher the water content, the larger the permanent axial strain. For the highest stress level, q_{max}=200 kPa, failure was observed in the test at a saturated state (TC3) during the first cycle (Fig. 13d). For the other tests, at a drier state, 900,000 cycles were applied for test TC1 (w=4%) and 600,000 cycles were applied for test TC2 (w=6%). Even with such a large number of cycles, stabilisation of the permanent axial strain was not observed at the end of these tests.

For further analysis of the effect of the water content and the stress level on the permanent axial strain, in Fig. 14, the values of cumulated permanent axial strain taken from the end of each stage are plotted versus the water content and the deviator stress. The results show that a linear relationship could be established between the final permanent axial strain and the water content for each stress level (Fig. 14a). For a given water content, the relationship between the final permanent axial strain and the deviator stress could be fitted by an exponential function (Fig. 14b).

5. Modelling the permanent axial strain

5.1. Background

Experimental results indicated that the stress state, the number of cycles, the soil physical state (soil water content and dry density), and the soil type are the major factors affecting the permanent strain under repeated loading (Li and Selig, 1996; Gidel et al., 2001). According to the results of triaxial tests, various empirical approaches have been proposed to predict the permanent deformation as a function of either the number of cycles (Barksdale, 1972; Paute et al., 1988; Sweere, 1990; Hornych et al., 1993) or the applied stress levels (Shenton, 1974; Lekarp and Dawson, 1998). Several models using the shakedown approach have been developed and applied in pavement design (Huurman, 1997; Theyse, 2000). On the whole, these models were elaborated based on cyclic triaxial tests with a single level of deviator stress in each test. With this procedure, determining the parameters for a model requires a large number of tests. This is obviously not realistic when performing large-scale triaxial tests on coarse-grained soils, because these tests are time-consuming and require a large quantity of materials. For this reason, multi-stage loading is usually recommended. Selig and Water (1994) have analysed the results of multi-stage loading tests on ballast and have observed the following phenomena:

- When the deviator stress exceeds the past maximum value, significant permanent strain occurs.
- For a given effective confining pressure, the loading sequence does not affect the final value of permanent strain when the total number of cycles at each stress level is the same.

Gidel et al. (2001) applied the same procedure when testing Unbound Granular Materials (UGM) and reached similar conclusions. They studied the permanent strain behaviour of two UGMs (0/20 limestone UGM and 0/10 UGM obtained from a micro-granite) following various stress paths with a $\Delta q/\Delta p$ ratio between 0 and 3. Based on the results obtained, they developed a new model relating the permanent axial strain to the maximum applied cyclic stress and the number of cycles (Gidel et al., 2001). The general form for this model was written as follows:

$$\varepsilon_1^p = g(\Delta p_{max}, \Delta q_{max}) f(N) \quad (1)$$

In the model of Gidel et al. (2001), the effects of the number of cycles and the maximum applied stress are separated, making it easier to determine these functions. For function $f(N)$, the model proposed by Hornych et al. (1993) was adopted (Eq. (2)). This model was verified and validated using the experimental results for UGMs. It has also been adopted in the French standard for cyclic triaxial tests (AFNOR, 1995).

$$f(N) = \varepsilon_1^{p*} = \varepsilon_1^p(N) - \varepsilon_1^p(100)$$

$$= A\left(1 - \left(\frac{N}{100}\right)^{-B}\right) \text{ (for } N > 100 \text{ cycles)} \quad (2)$$

where ε_1^{p*} is the permanent strain after the first 100 cycles, and A and B are regression parameters. A depends on the stress

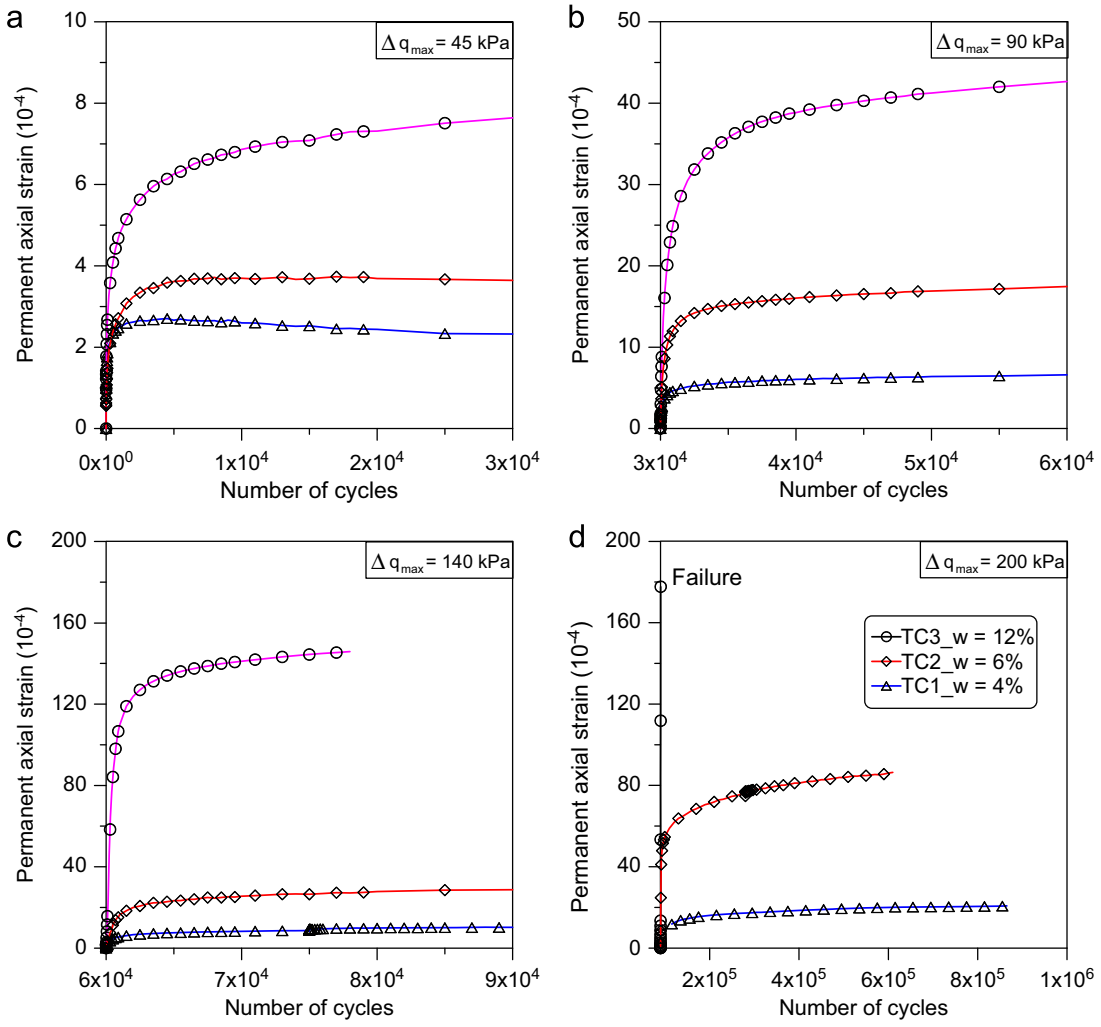

Fig. 13. Cyclic triaxial tests at three water contents: (a) first stage, q_{max}=45 kPa; (b) second stage, q_{max}=90 kPa; (c) third stage, q_{max}=140 kPa; (d) fourth stage, q_{max}=200 kPa.

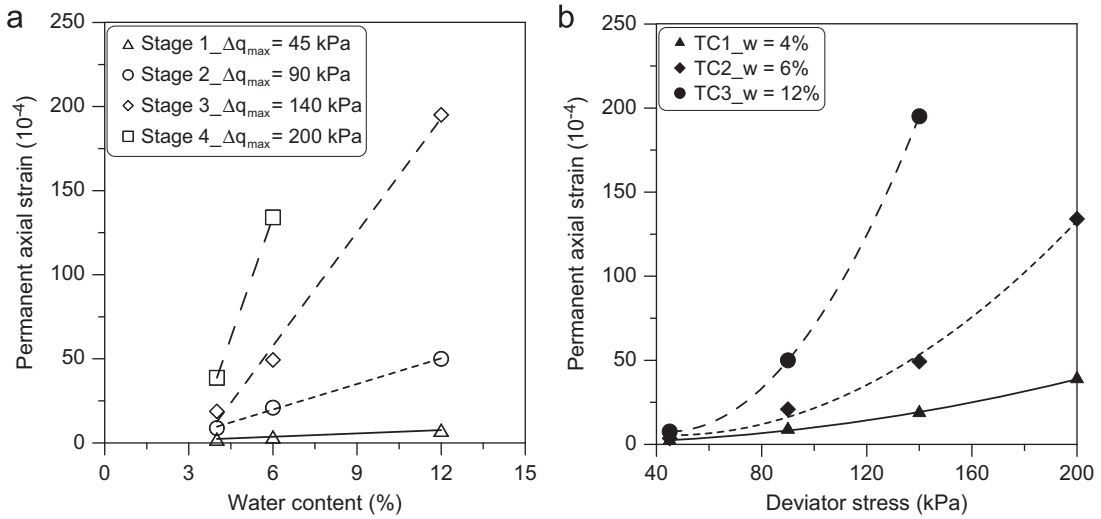

Fig. 14. Cumulated permanent axial strain recorded at the end of each loading stage versus (a) water content and (b) deviator stress.

level and the material; it represents the maximum permanent strain when the number of cycles tends toward infinity. B controls the evolution of permanent strain with the increase in cycle numbers. According to Gidel et al. (2001), this

relationship is valid only for $N > 100$ cycles, because the first one hundred loading cycles correspond to the bedding down of the material.

For function $g(\Delta p_{max}, \Delta q_{max})$, Gidel et al. (2001) showed that the permanent axial strain increases with the increase in mean stress p and that this increase in axial strain is highly dependent on the stress path defined by $\Delta q_{max}/\Delta p_{max}$. The relationship between the permanent axial strain and the maximum applied stress in the case of $q > 0$ is given below

$$g(\Delta p_{max}, \Delta q_{max}) = \varepsilon_1^{p0} \left(\frac{l_{max}}{p_a}\right)^n \frac{1}{\left(m + \frac{s}{\Delta p_{max}} - \frac{\Delta q_{max}}{\Delta p_{max}}\right)} \quad (3)$$

where ε_1^{p0}, m, n, and s are parameters, $l_{max} = \sqrt{\Delta p_{max}^2 + \Delta q_{max}^2}$, and $p_a = 100$ kPa.

The influence of the water content on the mechanical behaviour of granular materials under cyclic loading has been observed experimentally in several studies (Selig and Water, 1994; Gidel et al., 2002; Ekblad, 2006; Werkmeister et al., 2003). The results obtained in the present work on the fouled ballast have been found to be in agreement with these works. Nevertheless, to the authors' knowledge, the effect of the soil water content on the permanent strain has not been considered in the modelling. In the present study, the model proposed by Gidel et al. (2001) is modified in order to consider the effect of the water content.

According to the results shown in Fig. 14, a function relating the permanent axial strain to the water content and the applied deviator stress, $t(w, \Delta q_{max})$, can be established as follows:

$$t(w, \Delta q_{max}) = \varepsilon_1^{p0} \times (w + a) \times \left(\frac{\Delta q_{max}}{p_a}\right)^{\alpha} \quad (4)$$

where ε_1^{p0}, a, and α are parameters, and $p_a = 100$ kPa.

A comparison between Eqs. (3) and (4) shows that term Δp_{max} in Eq. (3) disappears in Eq. (4). This is because when the loading starts at $q = 0$ and the stress paths followed are $\Delta q/\Delta p = 3$, Δp_{max} is a function of Δp_{max}. In other words, Eq. (4) is only valid for the particular stress path considered. Further studies with more stress paths are needed to generalise this equation. In order to account for the stress level, the number of cycles, and the water content of the soil, Eq. (4) is extended as follows:

$$\varepsilon_1^p = t(w, \Delta q_{max}) \times f(N) \quad (5)$$

where $f(N)$ is calculated using Eq. (2) and $t(w, \Delta q_{max})$ is calculated using Eq. (4).

In this study, the measured data from tests TC1 ($w = 4\%$) and TC2 ($w = 6\%$) are used for determining the model parameters. These parameters are then used to simulate test TC3 (saturated state) in order to evaluate the performance of the proposed model. The parameters of the proposed model are determined by the following two steps:

- Step 1: Determine parameters ε_1^{p0}, a, and α by fitting Eq. (4) to the permanent axial strain at the end of each loading stage in tests TC1 and TC2, as shown in Fig. 15; the values obtained are $\varepsilon_1^{p0} = 9.14 \times 10^{-4}$, $a = -3.36$, and $\alpha = 2.54$.
- Step 2: Determine parameters A and B by fitting Eq. (5) to the results of tests TC1 and TC2; in Fig. 16, the fitting curves and the experimental results are shown. The parameters obtained are $A = 0.76$ and $B = 0.17$. Note that Eq. (5) is only fitted to the measured permanent axial strain when the number of cycles is larger than 100.

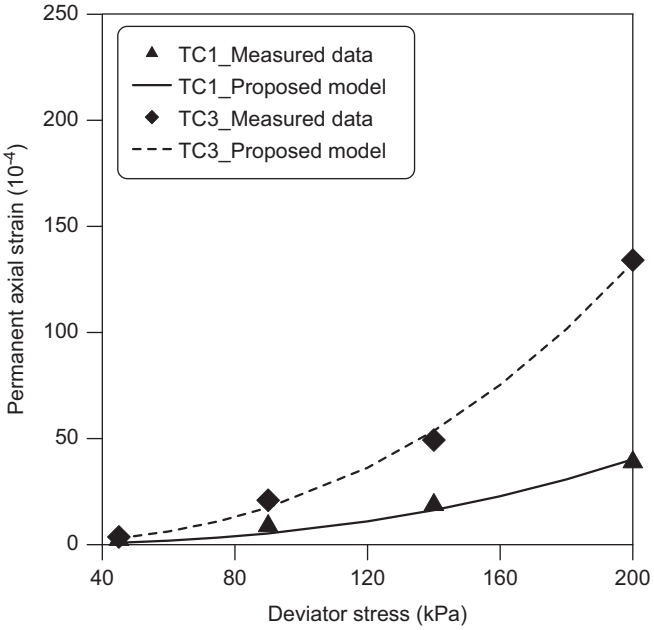

Fig. 15. Fit of cumulated permanent axial strain recorded at the end of each loading stage with the proposed model.

Fig. 16a shows that the proposed model fits well with the experimental results. For test TC1, in the last loading stage, the model value is close to the measured value at the end of the test. For test TC2, by contrast, a larger difference between the simulation and the experimental results can be observed in the last loading stage. Fig. 16b presents a zoom of the results for the first three loading stages. It is observed that the simulation of test TC1 is better than that of test TC2, i.e., a good match for test TC1, but not for test TC2. This is related to the final value of the permanent axial strain at the end of each loading stage. Indeed, it was observed that the stabilisation of the permanent axial strain occurred for test TC1, but not for TC2. Better simulation results can be expected if stabilised permanent axial strains are accounted for in the determination of the parameters.

The parameters of the model, thus determined, are then used to simulate test TC3 (saturated specimen). Fig. 17 presents a comparison between the experimental results and the simulation. It can be observed that the parameters determined from tests TC1 ($w = 4\%$) and TC2 ($w = 6\%$) enable a satisfactory simulation of test TC3 ($w = 12\%$) for the first two loading stages. Significant differences between

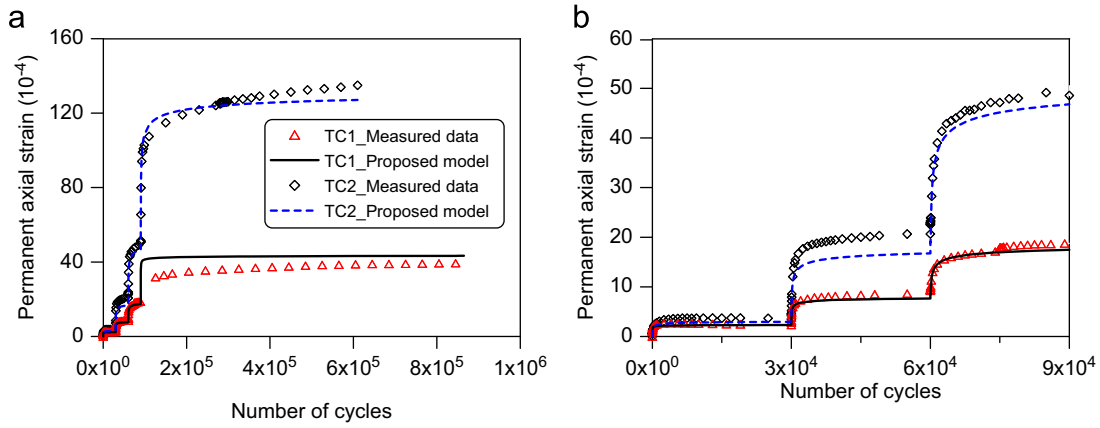

Fig. 16. Determination of parameters by fitting the experimental results of tests TC1 (w=4%) and TC2 (w=6%).

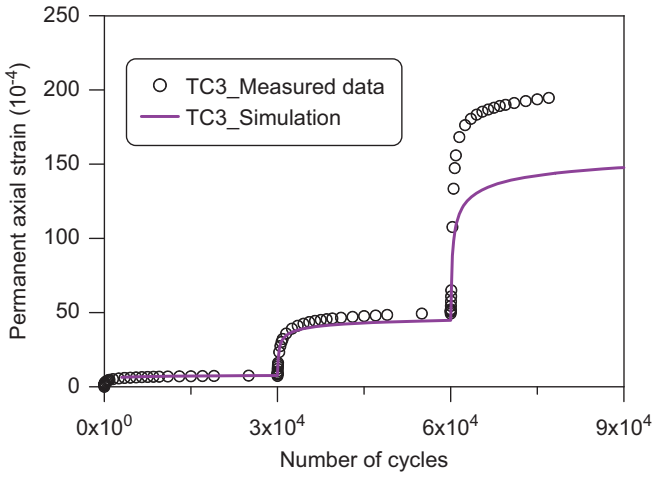

Fig. 17. Verification of the proposed model—simulation of test TC3 (saturated state).

the simulation and the results are observed, however, for the third loading stage that corresponds to large deformations ($\varepsilon_1^p > 150 \times 10^{-4}$).

The difference between the simulation and the results at high stress levels can be explained by the "shakedown theory" (Werkmeister et al., 2004; AFNOR, 2004; García-Rojo and Herrmann, 2005). Actually, there are three categories of material responses under repeated loading, plastic shakedown—category A (steady deformation behaviour), plastic creep—category B (failure at a large number of cycles), and incremental collapse—category C (failure at a small number of cycles). The critical stress levels can be defined according to the accumulated permanent axial strain. Following AFNOR (2004), the plastic creep limit is reached when $\varepsilon_{1\ 5000}^p - \varepsilon_{1\ 3000}^p > 4 \times 10^{-4}$ for UGMs, where $\varepsilon_{1\ 5000}^p$ and $\varepsilon_{1\ 3000}^p$ are the accumulated permanent axial strains at 5000 cycles and 3000 cycles, respectively. For fouled ballast, this value is 1×10^{-4} for TC1, 4×10^{-4} for TC2 in the last loading stage, and 5.6×10^{-4} for TC3, in the third loading stage. This shows that tests TC1 and TC2 are of categories A and B, respectively, at a deviator stress of q_{max}=200 kPa. At q_{max}=140 kPa, test TC3 exceeds the plastic creep limit (range C). An examination of Figs. 16 and 17 shows that the proposed model can only fit well with the permanent deformation of categories A and B. The influence of the water content on the permanent deformation and the shakedown limit of fouled ballast is significant. The critical shakedown load decreases with an increasing water content. This result is similar to that obtained by Werkmeister et al. (2003) on UGMs. According to the obtained parameters for the proposed model, there is no permanent axial strain of the fouled ballast when its water content is lower than 3%.

6. Conclusion

The aim of this study was to investigate the mechanical behaviour of the fouled ballast in the ancient railway track substructure under cyclic loading at various water contents. A large-scale triaxial apparatus was used to carry out both monotonic and cyclic tests on remould soil under constant water content conditions.

The monotonic triaxial tests were performed at two water contents, 4% (S_r=32%) and 12% (saturated state). The influence of the water content on the mechanical characteristics of the fouled ballast was found to be significant. The failure deviator stress at the water content of 4% was much higher than that of the saturated specimen. The friction angle was similar for the two water contents, while the apparent cohesion at the water content of 4% was significantly higher than that in the saturated state, i.e., 60 kPa versus 22 kPa.

The permanent deformation behaviour was studied by carrying out cyclic triaxial tests with large numbers of cycles. Three specimens having different water contents (4, 6, and 12%) were tested. The results showed that the permanent axial strains were larger for higher water contents.

In order to predict the permanent axial strain, a constitutive model accounting for the effects of the stress level, the number of cycles, and the water content of the soil was developed based on the results of cyclic triaxial tests with a multi-stage loading procedure and the model proposed by Gidel et al. (2001). The parameters were first determined by fitting the tests with water contents of 4 and

6%. The parameters determined were then used to simulate the test corresponding to the saturated state ($w=12\%$). The simulation was in good agreement with the experimental results, indicating the performance of the proposed model for the prediction of permanent deformation within the fouled ballast of categories A and B. Further study is necessary, however, to better describe the deformation behaviour of category C.

From a practical point of view, the results obtained in this study can be helpful in the assessment of ancient railway track substructure degradation. Indeed, such degradation occurs when changes in hydrological conditions at the site lead to changes in the water content of the fouled ballast, because the mechanical resistance of the fouled ballast can be sensitive to changes in the water content due to the presence of fine-grained soils in it. The results of the cyclic triaxial tests showed clearly that an increase in water content led to a significant increase in the permanent strain of the fouled ballast at the site of Sénissiat. The proposed model allows for the prediction of permanent axial strain, taking into account the effect of the water content. It can be used as a tool for assessing the sensitivity of the mechanical properties to changes in the water content. Once the sensitivity has been identified, appropriate measures can be taken to maintain the mechanical performance of the railway substructure, for instance, setting a drainage system to facilitate water evacuation or setting an impermeable layer on the fouled ballast layer to minimise water infiltration, etc.

Acknowledgements

This study was carried out within the research project "Track substructure without drainage—permeable structure". The authors would like to thank the Ecole des Ponts ParisTech (ENPC), the Railway Network of France (RFF), and the French National Railway Company (SNCF) for their support.

References

AFNOR, 1994. NF P94-074—Sols: Reconnaisance et essays. Essais à l'appeil triaxial de révolution.

AFNOR, 1995. NF P98-235-1—Test relating to pavements. Unbound granular materials. Part 1: Repeated Loading Triaxial Test.

AFNOR, 1999. NF P94-093—Sols: Reconnaissance et essays. Détermination des références de compactage d'un matériau.

AFNOR, 2004. EN 13286-7—Unbound and hydraulically bound mixtures, Part 7: Cyclic load triaxial test for unbound mixtures.

Alias, J., 1984. La voie ferrée—Techniques de construction et d'entretien. SNCF, Eyrolles.

Barksdale, R.D., 1972. Laboratory evaluation of rutting in base course materials. In: Proceedings of the Third International Conference on Structural Design of Asphalt Pavement, vol. 3, pp. 161–174.

Brown, S.F., 1974. Repeated load testing of a granular material. Journal of Geotechnical Engineering, ASCE 100 (7), 825–841.

Dupla, J.-C., Pedro, L.S., Canou, J., Dormieux, L., 2007. Mechanical behaviour of coarse grained soils reference. Bulletin de Liaison des Laboratoires des Ponts et Chaussées 268–269, 31–58 (N°).

Ekblad, J., 2006. Influence of water on coarse granular road material properties. Road Materials and Pavement Design 7 (3), 369–404.

Ekblad, J., 2008. Statistical evaluation of resilient models characterizing coarse granular materials. Materials and Structures 41 (3), 509–525.

Fortunato, E., Pinelo, A., Fernades, M.M., 2010. Characterization of the fouled ballast layer in the substructure of a 19th century railway track under renewal. Soils and Foundations 50 (1), 55–62.

García-Rojo, R., Herrmann, H.J., 2005. Shakedown of unbound granular material. Granular Matter 7 (2), 109–118.

Gidel, G., Hornych, P., Chauvin, J.J., Breysse, D., Denis, A., 2001. A new approach for investigating the permanent deformation behaviour of unbound granular material using the repeated load triaxial apparatus. Bulletin de Liaison des Laboratoires des Ponts et Chaussées 233, 5–21.

Gidel, G., Breysse, D., Denis, A., 2002. Influence de l'état hydrique et des sollicitations routières sur l'évolution du comportement des graves non traitées calcaires utilisées en assise de chaussée. Revue française de génie Civil 6 (5), 789–799.

Gräbe, P.J., Clayton, C.R.I., 2009. Effects of principal stress rotation on permanent deformation in rail track foundations. Journal of Geotechnical and Geoenvironmental Engineering 135 (4), 555–565.

Hornych, P., Corté, J.F., Paute, J.L., 1993. Etude des déformations permanents sous chargements répétés de trois graves non traitées. Bulletin de Liaison des Laboratoires des Ponts et Chaussées 184, 77–84.

Huurman, M., 1997. Permanent Deformation in Concrete Block Pavement. Ph.D. Thesis. Delft University of Technology.

Indraratna, B., Ionescu, D., Christie, H.D., 1998. Shear behavior of railway ballast based on large-scale triaxial tests. Journal of Geotechnical and Geoenvironmental Engineering 124 (5), 439–449.

Jain, V.K., Keshav, K., 1999. Stress distribution in railway formation—a simulated study. Pre-Failure Deformation Characteristics of Geomaterials. IS-Torino/Italy/1999, pp. 653–658.

Kalcheff, I.V., Hicks, R.G., 1973. Test procedure for determining the resilient properties of granular materials. Journal of Testing and Evaluation 1 (6), 472–479.

Lackenby, J., Indraratna, B., McDowell, G., Christie, D., 2007. Effect of confining pressure on ballast degradation and deformation under cyclic triaxial loading. Geotechnique 57 (6), 527–536.

Lekarp, F., Dawson, A., 1998. Modelling permanent deformation behaviour of unbound granular materials. Construction and Building Materials 12 (1), 9–18.

Li, D., Selig, E.T., 1994. Resilient modulus for fine-grained subgrade soils. Journal of Geotechnical Engineering 120 (6), 939–957.

Li, D., Selig, E.T., 1996. Cumulative plastic deformation for fine-grained subgrade soils. Journal of Geotechnical Engineering 122 (12), 1006–1013.

Li, D., Selig, E.T., 1998. Method for railways track foundation design—I: development. Journal of Geotechnical and Geoenvironmental Engineering 124 (4), 316–322.

Malla, R.B., Joshi, S., 2008. Subgrade resilient modulus prediction models for coarse and fine-grained soils based on long-term pavement performance data. International Journal of Pavement Engineering 9 (6), 431–444.

O'Reilly, M.P., Brown, S.F., 1991. Cyclic Loading of Soils. Blackie Book, pp. 477.

Paute, J.L., Jouve, P., Martinez, J., Ragneau, E., 1988. Modèle de calcul pour le dimensionnement des chaussées souples. Bulletin de Liaison des Laboratoires des Ponts et Chaussees 156, 21–36.

Pérez, I., Romana, M.G., Medina, L., 2006. Influence of stress levels on the development of permanent deformation in unbound granular materials. American Society of Civil Engineers, Shanghai, China, pp. 180–188.

Raymond, G.P., Williams, D.R., 1978. Repeated load triaxial tests on dolomite ballast. American Society of Civil Engineers, Journal of the Geotechnical Engineering Division 104 (7), 1013–1029.

Raymond, G.P., Bathurst, R.J., 1994. Repeated-load response of aggregates in relation to track quality index. Canadian Geotechnical Journal 31 (4), 547–554.

Selig, E.T., Water, J.M., 1994. Track Geotechnology and Substructure Management. Thomas Telford, London.

Shenton, M.J., 1974. Deformation of railway ballast under repeated loading triaxial tests. Soil Mechanics Section. British Railways Research Department, Derby, England.

SNCF, 2006. IN3278—Référenciel technique pour la réalisation des LGV—partie Génie Civil. Référentiel Infrastructure SNCF.

SNCF, 2009. R2520-2009-01—Sollicitations mécaniques dans la Plate-forme: Mesures d'accélérations verticales dans la plate-forme. Rapport technique de la SNCF.

Stewart, H.E., 1986. Permanent strain from cyclic variable-amplitude loadings. Journal of Geotechnical Engineering 112 (6), 646–660.

Suiker, A.S.J., Selig, E.T., Frenkel, R., 2005. Static and cyclic triaxial testing of ballast and subballast. Journal of Geotechnical and Geoenvironmental Engineering, ASCE 131 (6), 771–782.

Sweere, G.T.H., 1990. Unbound Granular Bases for Roads. Edited by D.U.o.T. Ph.D. Thesis. Delft, Netherlands, pp. 431.

Theyse, H.L., 2000. The development of mechanistic-empirical permanent deformation design models for Unbound Pavement Materials from laboratory and accelerated pavement test data. UNBAR 5, 285–293.

Trinh, V.N., Tang, A.M., Cui, Y.J., Canou, J., Dupla, J.C., Calon, N., Lambert, L., Robinet, A., Schoen, O., 2011. Caractérisation des matériaux constitutifs de plate-forme ferroviaire ancienne. Revue Française de Géotechnique 134–135, 65–74.

UIC, 2003. UIC 719R—Earthworks and track bed for railway lines. International Union of Railways.

Werkmeister, S., Numrich, R., Dawson, A.R., Wellner, F., 2003. Design of granular pavement layers considering climatic conditions. Transportation Research Record 1837, 61–70.

Werkmeister, S., Dawson, A.R., Wellner, F., 2004. Pavement design model for unbound granular materials. Journal of Transportation Engineering 130 (5), 665–674.

William, F.A., Peter, F., 2008. Behavior of railroad ballast under monotonic and cyclic loading. Journal of Geotechnical and Geoenvironmental Engineering 134 (3), 316–327.

Wolff, H., Visser, A.T., 1994. Incorporating elasto-plasticity in granular layer pavement design. Proceedings of the Institution of Civil Engineers: Transport 105 (4), 259–272.

Yang, L.A., Powrie, W., Priest, J.A., 2009. Dynamic stress analysis of a ballasted railway track bed during train passage. Journal of Geotechnical and Geoenvironmental Engineering, ASC 135 (5), 680–689.